Stable, Heat Conducting Phosphor Composites for High-Power Laser Lighting

Clayton Cozzan,[†,‡,¶] Guillaume Lheureux,[†,‡] Nicholas O'Dea,[‡] Emily E. Levin,[†,¶] Jake Graser,[§] Taylor D. Sparks,[§] Shuji Nakamura,[†,‡,‖] Steven P. DenBaars,[†,‡,‖] Claude Weisbuch,[*,†,‡] and Ram Seshadri[*,†,‡,¶,⊥]

†*Materials Department, University of California, Santa Barbara, California 93106, United States*

‡*Solid State Lighting and Energy Electronics Center, University of California, Santa Barbara, California 93106, United States*

¶*Materials Research Laboratory, University of California, Santa Barbara, California 93106, United States*

§*Department of Materials Science and Engineering, University of Utah, Salt Lake City, Utah 84112, United States*

‖*Department of Electrical and Computer Engineering, University of California, Santa Barbara, California 93106, United States*

⊥*Department of Chemistry and Biochemistry, University of California, Santa Barbara, CA 93106*

E-mail: weisbuch@engineering.ucsb.edu; seshadri@mrl.ucsb.edu

Abstract

Solid-state lighting using laser diodes is an exciting new development that requires new phosphor geometries to handle the greater light fluxes involved. The greater flux from the source results in more conversion and therefore more conversion loss in the phosphor, which generates self-heating, surpassing the stability of current encapsulation strategies used for light-emitting diodes, usually based on silicones. Here we present a rapid method using spark plasma sintering (SPS) for preparing ceramic phosphor composites of the canonical yellow-emitting phosphor Ce-doped yttrium aluminum garnet (Ce:YAG) combined with a chemically compatible and thermally stable oxide, α-Al_2O_3. SPS allows for compositional modulation, and phase fraction, microstructure, and luminescent properties of ceramic composites with varying compositions are studied here in detail. The relationship between density, thermal conductivity, and temperature rise during laser-driven phosphor conversion is elucidated, showing that only modest densities are required to mitigate thermal quenching in phosphor composites. Additionally, the scattering nature of the ceramic composites makes them ideal candidates for laser-driven white lighting in reflection mode, where Lambertian scattering of blue light offers great color uniformity and a luminous flux $>$1000 lm is generated using a single commercial LD coupled to a single phosphor element.

keywords: phosphor, laser lighting, solid state lighting, spark plasma sintering, white light

Keywords

phosphor, laser lighting, solid state lighting, spark plasma sintering, white light

1 Introduction

Solid state white lighting is more efficient than traditional sources and is currently experiencing increasing rates of adoption due to improvements in color quality and luminaire design. For high power lighting (>100,000 lumens) using light emitting diodes (LEDs), many diodes are required to produce high light output to avoid droop,[1] resulting in a luminaire with a very large footprint. Directional lighting using LEDs is limited by the emission angle for the emitter, requiring secondary optics that diminish the total light produced. To circumvent these technological and fundamental limits, laser diodes (LDs) provide a promising path forward owing to their monochromatic, highly coherent, and directional light emission.[2] LDs coupled to small inorganic phosphors allow very high luminous flux for a given solid state emitter,[3] and the small laser spot size can result in a quasi-point source of white light with a smaller étendue compared to conventional LED systems. New technologies, such as laser-boosted headlights[4] and visible light communication[5–7] have leveraged the benefits of LDs over LEDs. In these emerging demonstrations, a monochromatic LD is converted to broad band emission using inorganic phosphors. A key design requirement is the development of phosphor morphologies capable of withstanding high conversion and therefore high thermal loading due to the higher fluence from LDs.[8]

Despite impressive recent improvements in monochromatic LEDs and LDs, inorganic phosphors will likely always have a role in solid-state white lighting due to their ease to manufacture,[9] low cost compared to solid-state emitters, high efficiencies,[10] and well-studied emission and color stability with temperature. Thermal stability of phosphor emission is dictated by the crystal structure and the dopant concentration.[11] Lower efficiencies are observed at elevated temperatures for a given dopant concentration due to thermal quenching, and more quenching is observed as dopant amount in a phosphor is increased for a given temperature.[12] For example, the widely used yellow-emitting Ce-doped yttrium aluminum garnet (YAG) phosphor quenches at high temperatures partially due to thermal ionization,[13] which adds to heat generated *via* the Stokes shift.[10] These mechanisms raise

the phosphor temperature and degrade efficiency and color stability. LED phosphor encapsulation schemes impact the thermal conductivity of the phosphor element, such as an epoxy resin, silicone, or glass, that is mixed with the phosphor and then cured.[14] Therefore, to mitigate thermal quenching, the phosphor morphology used must have enough thermal conductivity to dissipate heat generated from conversion.

Many new strategies have been explored to improve the thermal conductivity of phosphor encapsulation schemes. Phosphor-in-glass, or the mixture of phosphor powders with glass frit at low temperatures, is reported to display higher thermal conductivity to $2.18\,\mathrm{W\,m^{-1}\,K^{-1}}$, but reflection losses of the excitation light led to a lower luminous efficacy than in silicone-based commercial white LEDs.[14,15] Thermally robust phosphors can be achieved by avoiding low thermal conductivity encapsulating materials altogether to create stand-alone phosphor monoliths, such as single crystals[16] or dense monolithic or composite ceramics[17–20] and have been successfully deployed in industry.[21] When compared to phosphors in silicone, polycrystalline ceramics offer control of light scattering *via* pore size and compositional tuning, reduced degradation, reduced color over angle shift, can be characterized before use with LEDs, and offer better heat conduction.[22] In addition to monolithic phosphor ceramics, phosphor composites (phosphors or multiple phosphors with heat dissipating materials) offer design flexibility.

In the present work, a series of Ce:YAG and α-Al_2O_3 composites were made using spark plasma sintering (SPS) and their phase fraction, microstructure, and luminescent properties ew studied for use in LD-based white lighting. Both transparent and scattering YAG[17,23,24] and YAG composites[19,25–29] have been studies previously for white light generation, the latter offering increased thermal conductivity and increased light extraction through the inclusion of alumina, which has a thermal conductivity three times that of YAG. For the first time, relationships between ceramic density, thermal conductivity, and operating temperature are investigated and reveal that large differences in thermal conductivity as a function of Al_2O_3 do not translate to significantly lower operating temperatures

for the system design studied presently. Unique experimental insights into the relationship between density, thermal conductivity, and operating temperature demonstrate that encapsulation-free composites of modest density do not sacrifice light output ($>$1000 lm for one phosphor and one LD) with naturally Lambertian scattering of incoming laser light rendering a more uniform white light. Additionally, the composites sufficiently mitigate thermal quenching and are superior to ceramics containing no alumina, offering high light output and excellent color uniformity with no additional preparation.

2 Methods

Mixtures of commercially available Ce-doped yttrium aluminum garnet ($Y_3Al_5O_{12}$:Ce^{3+} or Ce:YAG) and alpha phase alumina (α-Al_2O_3 average particle size of 0.71 μm, Materion, 99.9%) were prepared *via* mixing with an agate mortar and pestle with care taken to mix and not grind the powders, in the following amounts: 25%, 50%, 75%, and 100% by weight Ce:YAG respectively. Samples were densified using the spark plasma sintering technique in an FCT Systeme GmbH SPS furnace. Powders were placed in a graphite die of 10 mm diameter with 1 mm thick graphite foil lining the die. The sample chamber was pumped down to vacuum with a preload of 3 kN applied, and subsequently increased to 5 kN or 8 kN over 30 s once vacuum was achieved. The sample was heated up to 1200–1500°C at a rate of 200°C min^{-1} with a 5 min hold, and then finally cooled to room temperature in over 10 min. The resulting samples were then sanded to remove the graphite foil. The maximum temperature was increased with increasing Ce:YAG content as Ce:YAG was observed to densify at a higher temperature than the Al_2O_3.

Sintered samples were annealed using a Lindberg tube furnace with an alumina tube under 0.1 L min^{-1} of 5% H_2:95% Ar with the following heating regimen; a 2 °C min^{-1} heating to 1500 °C, 24 h at 1500 ° C, and finally a 2 °C min^{-1} cool to room temperature. Geometric density was measured before and after annealing by weighing the samples and

measuring their dimensions using a micrometer. Density of the samples was not altered by the annealing step. Qualitative information on carbon concentration as a function of depth was obtained using secondary ion mass spectrometry (SIMS). SIMS was performed on a Cameca IMS-7f Auto system using Cs primary ions. A gold coat and electron flood were used to control electrical charging effects. In each sample, three 100 μm craters were made, and secondary ions were collected from the center 33 μm. The etch rate was approximately 65 nm min^{-1}, and composition down to a depth of 2500 nm to 3000 nm was investigated. Aluminum ions (^{27}Al) were collected in addition to carbon, for purposes of normalizing the carbon results across samples.

X-ray powder diffraction was performed at room temperature using a Panalytical Empyrean powder diffractometer with Cu $K\alpha$ radiation. Starting materials and powder from grinding sintered samples with an agate mortar and pestle were was placed on a zero background silicon holder and scanned for an 1 h in duration. Rietveld refinement of the diffraction data was performed using the General Structure Analysis System (GSAS) with EXPGUI.[30,31] Scanning electron microscopy (SEM) images of the sintered samples were collected using a FEI XL30 Sirion FEG Scanning Electron Microscope using a backscattered electron detector for compositional contrast with a 15 kV beam voltage.

Photoluminescence spectra were collected using a 50 cm diameter integrating sphere with a commercial blue laser diode in a copper heat sink mounted in a side port and the phosphor sample mounted in the center of the sphere. The diode was controlled by a Keithley 2440 5A SourceMeter. Data were collected using a MAS40 spectrometer with a 2.0 OD filter. A correction factor was experimentally measured to account for the attenuation imparted by the filter. Quantum yield (QY) was calculated using a two measurement approach.[32] To mitigate sample heating for phosphor powders measured in silicone, a 1.0 OD filter was placed in front of the LD to attenuate the LD light. No filter was required for ceramic samples. The data collected was then used to calculate optical properties, such as quantum yield and luminous flux, using Mathematica. Current, voltage, radiometric, and

electrical power used to calculate wall plug efficiency (WPE) for the LD used is shown in Supporting Information (Figure S1). For phosphors measured in silicone, phosphor powders were thoroughly mixed at 25 wt% in a silicone matrix (Momentive, RTV-615) using a high speed mixing system (FlackTek Inc., DAC 150.1 FVZ-K) at 1500 rpm for 5 min and subsequently deposited on a 100 mm^2 fused silica substrate and heated at 398 K for 15 min in a box furnace to accelerate the curing process.

Using the same commercial LD, samples were placed on a large aluminum heat sink and monitored using a FLIR A310 thermal imaging camera with range 0°C–360°C. The LD lens was placed 5 cm away from the surface of samples at an angle of 45 °. The LD was mounted in a cylindrical copper heat sink of diameter 20 mm to mitigate laser overheating. The samples were placed on a large metal heatsink that was much larger in volume than the sample and thermally attached using a silicone-based thermal joint compound. The samples were then monitored using an infrared (IR) camera. Emissivity of the samples was set to 0.95 to obtain the temperature from IR camera images.

Thermal diffusivity was measured using the laser flash technique between room temperature and 973 K under an argon atmosphere on a Netzsch LFA 457 system with a flow rate of 100 ml min^{-1}. Pellets for the measurement, approximately 6 mm in diameter and 2 mm thick, were sprayed with a layer of carbon paint to minimize errors in the emissivity. Heat capacity was calculated using a Netzsch DSC 3500. The samples were run from 273 K to 773 K and back under nitrogen gas. The energy required to heat the samples were compared to a sapphire standard using a inbuilt ratio method. The thermal conductivity was calculated using $\kappa = \alpha C_p \rho$, where α, C_p, and ρ are the thermal diffusivity, heat capacity, and density, respectively.

To characterize reflection of incoming laser light and analyze the color uniformity, angular resolved experiments were carried out on a home-built system. A commercial LD was mounted and used to excite samples at an incident angle of 30 °. Samples were placed on a heat sink while a an optical fiber attached to a mechanical arm scanned angles from

0 ° to 90 °. Light was collected using an optical fiber connected to a Horiba Jobin Yvon Spex 550 Triple Imaging Axial spectrometer.

3 Results and discussion

Ceramic phosphor composites of Ce:YAG and Al_2O_3 in different ratios by weight were prepared by mixing and densifying powders using SPS. SPS relies on graphite and carbon-based tooling surrounding the powder, resulting in a carbon-rich densification environment. After densification, the samples appeared dark in color due to the presence of carbon instead of yellow Ce:YAG and white Al_2O_3. Carbon contamination in SPS-prepared transparent oxides was observed by others, evidenced by lower in-line transmission.[33] The densified ceramics in the present work were then subjected to an annealing step in a reducing atmosphere of 0.1 L min^{-1} of 5% H_2:95% Ar for 6 h at 1500°C on an alumina crucible in an alumina tube furnace. It was hypothesized that heating in a reducing environment would mitigate carbon contamination as hydrogen is an effective etching gas for carbon.[34] Visually, the samples appeared closer to the color of the original starting powders after the annealing step (Fig S2). To investigate the effect of the annealing step on the amount of carbon in the ceramics, SIMS was performed on three craters 3 μm to 4 μm deeper than the surface of the samples, with areas of approximately 30 mm^2 assessed. Using ^{27}Al as a reference signal, it was confirmed by SIMS that an order of magnitude less carbon was present in the annealed sample than in the as-prepared by SPS with no anneal (Figure S3). All further investigations in the present work were performed on annealed ceramic samples.

No intermediate phases are expected when mixing and heating Ce:YAG ($Y_3Al_5O_{12}$) and Al_2O_3 to 1500°C, as evidenced by the α-Al_2O_3 and Y_2O_3 phase diagram.[35] To confirm the purity of phases in the sintered ceramics, X-ray diffraction was performed on powder derived from grinding an SPS-prepared ceramic sample (25% Ce:YAG and 75% Ce:YAG shown in Figure S4). Rietveld refinements of a representative 50% Ce:YAG ceramic ground

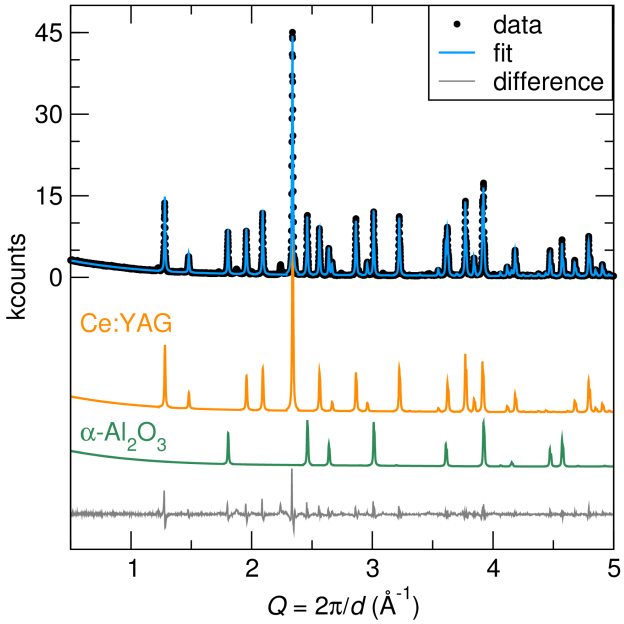

Figure 1: Rietveld refinement of powder from an SPS-prepared 50% Ce:YAG nominally by weight composite sample is shown with the components of Ce:YAG and α-Al_2O_3 displayed beneath. Results of the refinements indicate phase fractions of 48.6% Ce:YAG and 51.4% Al_2O_3, providing evidence to the compatibility of the two materials.

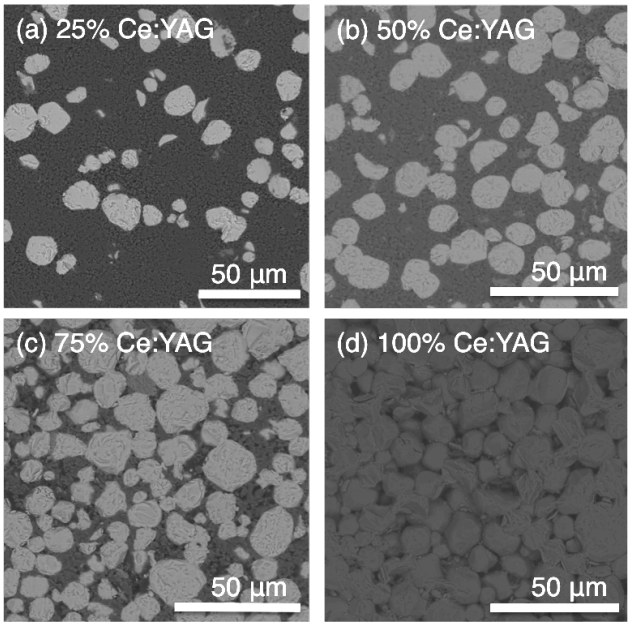

Figure 2: Backscattered SEM images show compositional contrast with lighter Ce:YAG and darker α-Al_2O_3 for the 25% (a), 50% (b), 75% (c), and 100% (d) Ce:YAG samples. Composite microstructures show Ce:YAG particles surrounded by a connected network of α-Al_2O_3.

into a powder (Figure 1) were used to obtain phase fractions, which were calculated to be 51.4% Al_2O_3 and 48.6% Ce:YAG. A table of refined unit cell parameters and refined atomic positions are shown in the Supporting Information in Table S1 and Table S2, respectively. The compatibility of $Y_3Al_5O_{12}$ and Al_2O_3 was also observed using SEM, where micrographs show Ce:YAG particles ($\sim 50\,\mu$m) distributed in an Al_2O_3 (0.71 μm) matrix (Figure 2). The particles of Ce:YAG isolated in the α-Al_2O_3 matrix suggest implications for both light scattering and thermal conductivity that will be discussed in more detail later in the present work. In Ce:YAG/Al_2O_3 phosphor systems, it has been noted that the refractive indices of YAG and Al_2O_3 are similar, potentially reducing backscattering and total internal reflection losses at crystal boundaries as an increased optical path enables more efficient excitation.[36] Additionally, higher thermal stability during conversion is also expected due to this morphology,[20] as the connectivity of the Al_2O_3 offers a percolating pathway for heat dissipation from Ce:YAG particles through the higher thermal conductivity of α-Al_2O_3.

Table 1: Coordinated color temperature (CCT), Commission Internationale de l'Éclairage (CIE) (x, y) coordinates, and color rendering index (CRI) of ceramic composites prepared using SPS with systematically increasing amounts of Ce-doped YAG phosphor. The 50% Ce:YAG ceramic shows CIE coordinates closest to the white point with lowest CCT.

	25%	50%	75%	100%
CCT (K)	12399	5340	6760	5872
CIE (x, y)	(0.29, 0.25)	(0.34, 0.32)	(0.32, 0.28)	(0.33, 0.31)
CRI	63	61	63	63

Emission properties for samples with varying wt% Ce:YAG were measured using an integrating sphere and a commercial laser diode and are reported in Table 1. In the present work, ceramic samples of 50% Ce:YAG measured the lowest coordinated color temperature (CCT), Commission Internationale de l'Éclairage (CIE) coordinates closest to the white point, and relatively low CRI that is to be expected for a blue LD source coupled with a yellow-emitting phosphor.[3,37] The LD was controlled using a Keithley 2440 power source with the LD operating at low power for $<$1000 ms to avoid sample heating. Small differences in the emission color of the ceramic phosphors did not follow any systematic trends.

Recent work on Ce:YAG/Al_2O_3 ceramics observed systematic blue-shifted emission as the amount of α-Al_2O_3 was increased.[29] It is therefore possible that the addition of α-Al_2O_3 mitigates the effects of reabsorption of the scattered blue light, resulting in blue-shifted emission with increasing α-Al_2O_3 content. However, this was not observed with consistency in the current work. Alternatively, as more α-Al_2O_3 is added to the system, less blue incident light is absorbed which may also result in the blue shift in emission. Therefore, it is difficult to conclude with confidence if differences in the emission spectra of 1-2 nm are due to the experimental setup or due to changes in light propagation as a function of α-Al_2O_3 content. As seen in the present work and in work by others,[29] white light near the white point (0.33, 0.33) can be achieved with 50% Ce:YAG samples. For these ceramics to be *via*ble white lighting devices, both color and efficiency must be considered, and the theoretical limit of phosphor quantum yield must be understood. Reported external quantum efficiencies in these systems are less than the Ce:YAG powder by itself,[20] possibly due to low extraction in the ceramics.

Table 2: PLQY measured for commercial Ce:YAG, a mixture of 50%Al_2O_3/50%Ce:YAG by weight, a 50%Ce:YAG ceramic, and powder achieved from grinding a 50%Ce:YAG ceramic. QY shows an initial drop from mixing with α-Al_2O_3, and a further drop in QY after SPS processing, due largely in part to the presence of carbon.

Sample	PLQY (%)	CIE (x, y)
Commercial Ce:YAG	*83–89	(0.33, 0.35)
50%Al_2O_3/50% Ce:YAG starting powders	*77–86	(0.27, 0.19)
50% Ce:YAG ceramic	*69–75	(0.29, 0.27)
97% theoretical density	48–53	

*indicates sample in silicone

For transparent Ce:YAG ceramics, the quantum efficiency of the transparent ceramics were reported to be lower than Ce:YAG powder due to waveguiding and backward emission losses.[38] In translucent or scattering Ce:YAG ceramics however, pores introduce scattering and can be controlled by tuning both the pore size and the prevalence of pores.[39] This scattering can overcome light trapping effects of the high index (n=1.85 at 450 nm)

in Ce:YAG.[40] In the present work, scattering is introduced both through the grain boundaries of the hexagonal Al_2O_3 mixing with cubic Ce:YAG, as well as the presence of pores. QY was measured for ceramic samples as-prepared using SPS, and the SPS samples were then ground into powders and mixed in silicone and measured. Curiously, the measured QY of the powders in silicone derived from grinding the ceramics (69-75%) was higher than the ceramics prior to grinding (48-53%), which could be due to increased extraction by using silicone due to different indices of refraction or an increase in the probability for reabsorption in the silicone sample.

In the present work, phosphor mixtures were investigated both prior to SPS and post SPS preparation to determine if the drop in photoluminescent quantum yield (PLQY) is due to processing. For the starting Ce:YAG powder, the PLQY of the commercial Ce:YAG in silicone was measured to be 83–89%, which matches expected values for this particular phosphor. A sample of 50% by weight Ce:YAG and 50% by weight Al_2O_3 in silicone measured a small drop in the PLQY to 77–86 % (Table 2). PLQY was measured using an integrating sphere setup reported elsewhere,[3] where the ranges reported presently are minimum and maximum values measured for a range of laser powers tested. In the current work, conclusions about PLQY across the range of ceramic samples prepared are difficult to make as the samples contain qualitative but not quantifiable amounts of carbon, which is known to absorb light.[41,42] Quantitative values for carbon concentration in the present samples are also very difficult as oxide and carbon standards for these ceramic oxides do not exist at the time of publication for methods such as SIMS. While the potential interplay between PLQY and density are difficult to elucidate in the present work, it is clear that SPS processing in a carbon rich atmosphere introduces carbon that lowers the PLQY of the composite ceramic phosphors. Future work is needed to decrease the presence of carbon to increase the PLQY.

The increase in extraction by encapsulating the phosphor powder in silicone might also provide some reasoning as to the lower QY observed in the ceramics than the original

powder, as some light might scatter but not escape the ceramic. However, the drop in QY observed is due largely to the carbon introduced *via* the SPS process. Other methods for preparation of ceramics, such as tape casting[43] and floating zone growth,[36] might provide a more viable route for higher purity ceramic phosphors in the future, and ceramics with higher QY values have been reported for Al_2O_3/Ce:YAG samples.[20] The rest of the current work will instead focus on the viability of this system for use in high power white lighting, with the knowledge that improvements in QY are possible *via* cleaner processing routes and more efficient starting phosphors.

The luminous flux (Φ_{lum}) is the light power of a white light emitting device as perceived by the human eye, and is given as follows (Eq. 1):

$$\Phi_{\mathrm{lum}} = 683\frac{\mathrm{lm}}{\mathrm{W}}\int_{\lambda} V(\lambda)S(\lambda)d\lambda \tag{1}$$

where 683 lm W^{-1} is a normalization factor representing the amount of lumens (lm) given by a light source of 1 W emitting at 555 nm, $S(\lambda)$ is the power spectral distribution measured experimentally, and $V(\lambda)$ is the eye response function which represents the intensity of color perception. One lumen is equal to a light source emitting one candela uniformly across a solid angle of one steradian. Therefore, luminous flux is the perceived total light output for a given emitter and phosphor combination or device and does not contain any information about the color of the light, just the intensity as perceived by the human eye. The luminous efficacy of radiation (LER), which is the luminous flux divided by the radiometric/optical power of the source (lm $W_{rad}{}^{-1}$), provides information about how efficiently visible light is produced by a given source. This is the upper limit measurement for a given light source and phosphor combination, whereas the overall luminous efficiency, calculated by dividing the flux by the electrical power of the solid state emitter, provides a measure of the actual device efficiency for producing light. Luminous efficiency is measured in lm $W_{elec}{}^{-1}$, and in the case of LED or LD based devices, is dictated by both the efficiency of electricity to light conversion (wall plug efficiency or WPE) and the efficiency

of the phosphor. For comparison, compact fluorescent light bulbs and fluorescent light tubes have luminous efficiencies around 50 lm W_{elec}^{-1} to 80 lm W_{elec}^{-1}.[44]

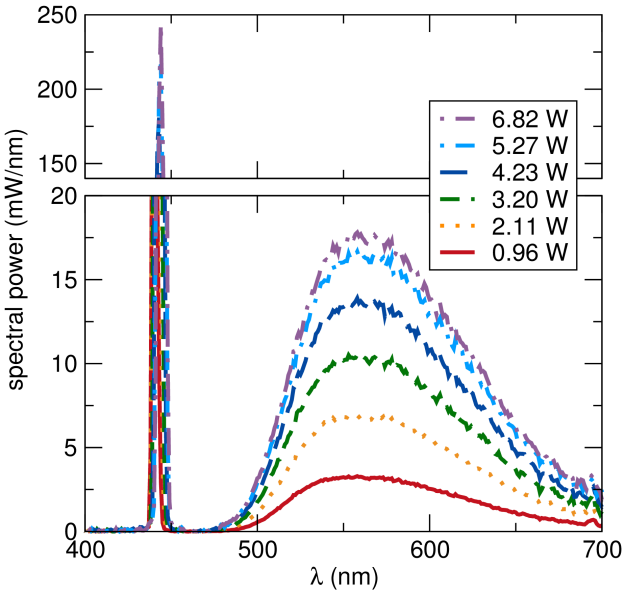

Figure 3: Spectral power distribution for increasing LD radiometric power for white light created when a 450 nm LD is incident a 50% Ce:YAG ceramic. White light is generated regardless of laser power, (0.34, 0.33) for 0.92 W_{rad} and (0.34, 0.32) for 6.82 W_{rad}.

Photopic parameters of the scattering Al_2O_3/Ce:YAG ceramics were measured as a function of radiometric laser power. In Figure 3, spectral power (mW nm^{-1}) of a 50% Ce:YAG ceramic is shown as a function of wavelength for different input powers of the blue LD. The spectral power reaches nearly 17 mW nm^{-1} for phosphor emission, which is a factor of twenty increase from earlier examples of LD-excited Ce:YAG for lighting.[37] Increases in spectral power observed in the present work are due to both higher performing lasers and thermally stable phosphor morphologies capable of withstanding high flux. At the maximum measured LD output power of 6.82 W, ~1.2 klm of white light was measured using an integrating sphere. Using only one phosphor sample and one commercial LD operating at maximum laser power, the 1.2 klm white light has a luminous efficacy of 165 lm W_{rad}^{-1} with a CRI of 65, CCT of 5350 K, and CIE coordinates of (0.34, 0.32). The luminous efficiency was measured to be 51 lm W_{elec}^{-1} using a 28% WPE LD. The most efficiency 50% Ce:YAG sample with measured density of 80% theoretical was PLQY=70%. These

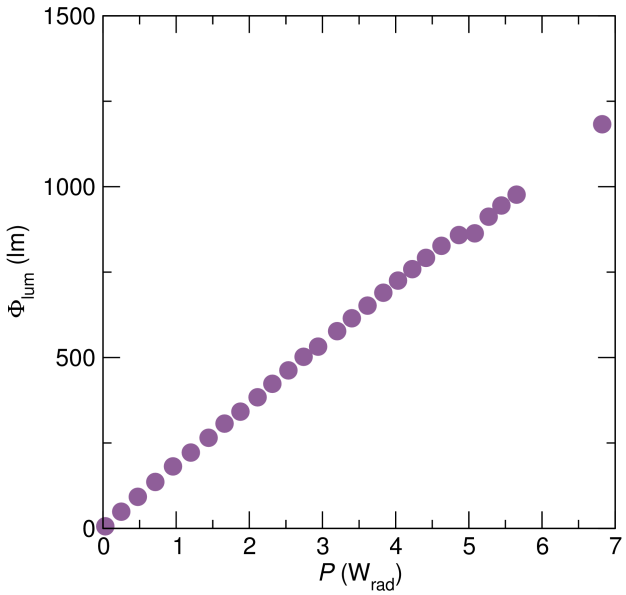

Figure 4: Luminous flux (Φ_{lum}) as a function of LD power for a 500% Ce:YAG ceramic, where a Φ_{lum} of 1.2 klm is observed at 6.82 W_{rad}.

luminous flux values are generally better than what is reported for the best single chip LEDs under normal operating conditions. The present demonstrations show that more than 1000 lm of white light can be produced by a single phosphor and a single solid state emitter. Since the above measurements were made with excitations $<$1 s, thermal management of the phosphors during operation must first be considered to understand feasibility for steady-state at high power. Additionally, it follows there is potential for increasing luminous flux *via* using multiple lasers for excitation, where thermal management is critical as roughly 25% of power is converted to heat due to Stokes shift and QY losses in the present system.

Densities of the samples were calculated using a weighted average of each component based on the nominal composition. To investigate the relationship between density and thermal conductivity, thermal diffusivity and heat capacity were measured from 323 K to 723 K to calculate thermal conductivity. Thermal conductivity as a function of temperature for a 100% Ce:YAG ceramic, a 50% Ce:YAG ceramic of similar density, and 50% Ce:YAG ceramics of increasing density are shown in Figure 5. It can be seen that for a similar

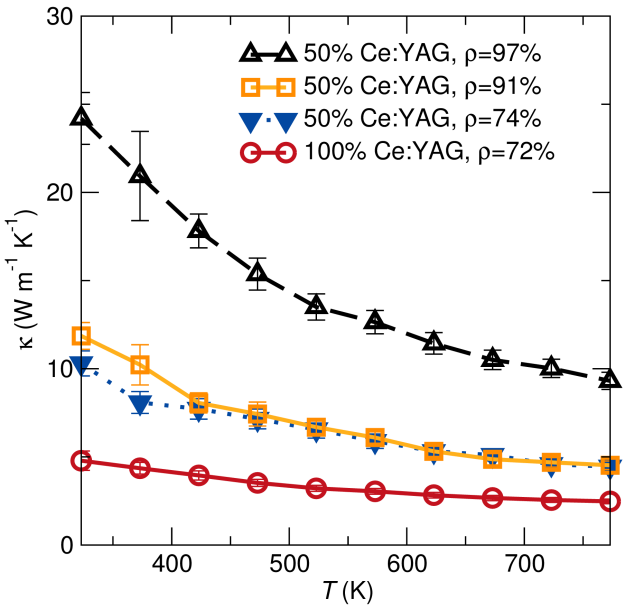

Figure 5: Thermal conductivity as a function of temperature from 323 K to 723 K for different ceramic samples shows that including Al_2O_3 increases thermal conductivity in the Ce:YAG/Al_2O_3 ceramics, and increasing density increases thermal conductivity. Density is listed after the sample composition. As expected, the 50% Ce:YAG ceramic with the highest density has the highest thermal conductivity.

theoretical density, the thermal conductivity at 323 K of a 100% Ce:YAG ceramic doubles with the inclusion of 50 weight % α-Al_2O_3. Thermal conductivity at 323 K continues to increase with increasing density. However, the current ceramics have QY values lower than typical values reported for Ce:YAG phosphors.[9] During conversion, more heat will be generated in the present ceramics due conversion losses due to the lower QY. The higher thermal conductivity of α-Al_2O_3 ($33\,W\,m^{-1}\,K^{-1}\pm2$)[45] compared to $9.2\,W\,m^{-1}K^{-1}$ for Ce:YAG[16] allows for a lower operating temperature at a given device current, which results in high conversion efficiency and higher luminous output at the same operating conditions due to reduced thermal quenching. This also allows for higher power density without reaching a thermal quenching or degradation regime.[22]

In the current work, benefits of the high thermal conductivity α-Al_2O_3 compete with the deleterious effects of porosity. It has long been known that both volume fraction of porosity and the size, shape, and orientation of the pores play a large role in the thermal

conductivity of ceramics.[46] The change in thermal conductivity for a given temperature in the current work is similar to observed values for alumina with an increase of 5-10% porosity resulting in a 5-10 $W\,m^{-1}\,K^{-1}$ drop in thermal conductivity,[46] which is directly related to the pore volume fraction in the composite materials. However, this is not observed to greatly impact the steady state temperature for the current configuration.

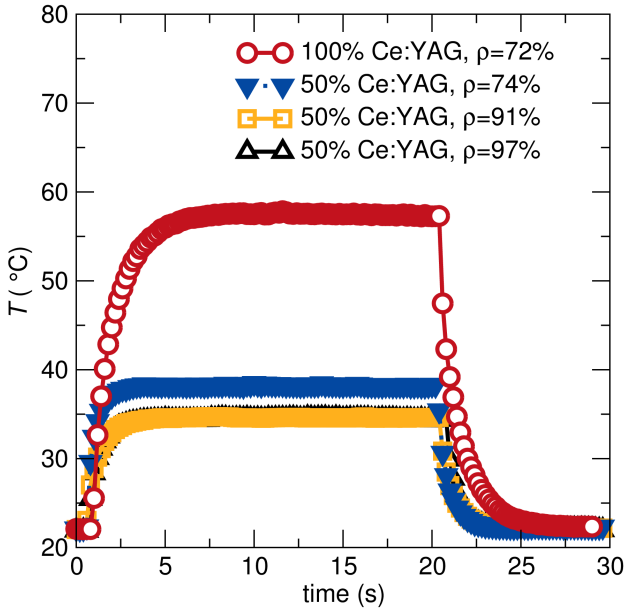

Figure 6: Heating curves of the ceramic samples and a Ce:YAG single crystal when excited by 5 W_{opt} of 450 nm LD excitation are shown. Including alumina in the ceramic phosphors lowers to saturation temperature to around the same value for densities ranging from 74% to 97%. All ceramic samples had the same dimensions and were affixed to a large metal heat sink using a thermal joint compound. Density of each ceramic is listed in legend.

To test the thermal management of the ceramic composites during LD excitation, samples were irradiated using a commercial laser diode with λ_{ex}=450 nm at 5 W_{rad}. The maximum surface temperature as a function of time is shown in Figure 6. There is a great reduction in steady-state temperature from 57 °C to 37 °C by including alumina in the composite for a given density, which is enough to prevent thermal quenching for the Ce:YAG doping concentration investigated presently.[11,12] There is only a difference in steady-state temperature of roughly 3 °C between ceramic composites with density of 74% and 97%, despite the large differences in thermal conductivity (Figure 5). While the amount of heating de-

pends on a large number of phosphor and device-specific parameters such as the thermal conductivity, the QY of the phosphor, the size of the sample, how it is thermally fixed to a heat sink, etc., the present results demonstrate that a baseline level of thermal conductivity is achieved using α-Al_2O_3 that successfully mitigates phosphor heating. Additionally, less phosphor material results in less heating without an appreciable loss in luminous flux (1180 lm for 100% Ce:YAG and 1023 lm for 50%Ce:YAG). In the current work, all samples are the same cylindrical shape with identical dimensions of 8 mm diameter and 2 mm thickness. For LD-based white lighting, small samples are preferred as it can be used as a quasi-point source. As sample volume decreases, the differences in thermal conductivity will likely play a larger role due to less thermal mass. However, it is observed in the current work that large increases in thermal conductivity are accompanied by small changes in the steady state temperature. Therefore, Ce:YAG/Al_2O_3 composites mitigate temperature very well whilst converting laser light even if the densities achieved are not the theoretical maximum.

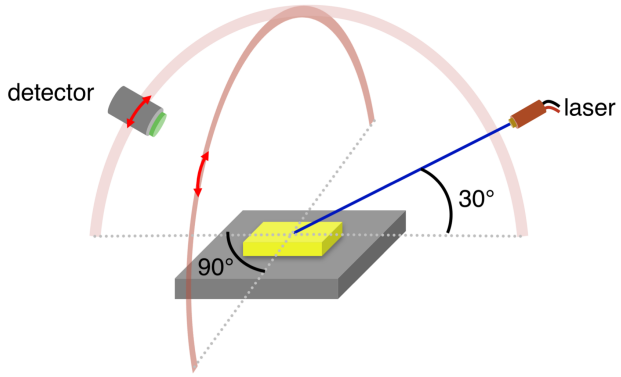

Figure 7: Scheme for measuring the angular dependence of light emission. The blue laser diode is fixed at an angle of 30°, relative to the sample surface while a detector attached to a goniometer arm is scanned along longitudes from 0°, to 180°, (scan directions indicated by the double arrows). First, the detector is scanned from 0° to 180° in the same plane as the laser diode, which is denoted as the 0° azimuthal scan in the data. Longitudinal scans at azimuthal angles of 45° and 90° with respect to the plane of the laser were also carried out. The longitudinal detector arc at an azimuthal angle of 90° is indicated.

One additional consideration for ceramic composites their scattering behavior, as the reflected light will play a role in both the color of a device as well as device safety. A recent

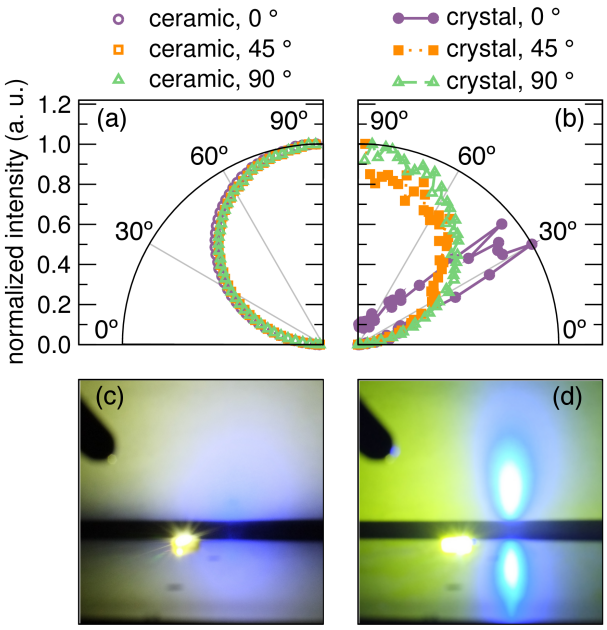

Figure 8: Normalized emission intensity for 375 nm to 525 nm emission is shown in (a) for a Ce:YAG/Al_2O_3 ceramic composite (open shapes) and in (b) for a roughened Ce:YAG single crystal (closed shapes connected with lines). The samples were excited by a blue LD at 30° incident to the sample surface, and the data is shown as a function of $\cos(\theta)$. Data for azimuthal detector angles of 0°, 45°, and 90° relative to the laser path are shown. The ceramic composite sufficiently scatters blue light rendering a uniform white color, as shown quantitatively by the isotropic luminance (a) and qualitatively in the photograph (c). The roughened single crystal reflects blue light at with the same angle as the incident LD (b), which leads to nonuniform emission (d).

study of this system hypothesized that the use of α-Al_2O_3 introduced additional scattering, resulting in altered light propagation and increased extraction efficiency, whereas transparent samples waveguide light *via* total internal reflection.[27] In the present work, angular dependent emission was collected for a 50% Ce:YAG ceramic sample as prepared *via* SPS with a rough surface and a commercially prepared Ce:YAG single crystal that is roughly the same volume using a home-built system described in Figure 7.

A polished surface reflects light away at the same angle as the incident light, meaning the reflected angle and incident angle are equivalent, and is known as specular reflection. A rough surface will reflect the light at more than one angle but predominantly in the same direction as the polished surface. For LD-based lighting in a reflection geometry, a matte surface might be preferred for color mixing, as blue source and yellow emitted light must mix to create white. Perfectly matte surfaces diffusely scatter light resulting in the same apparent brightness in every direction. While phosphor materials exhibit omnidirectional emission for the light that is absorbed and emitted, scattering of the incident light is an important consideration for making reflection-based devices.[47] In the present work, the reflection geometry is investigated as a demonstration that leverages the highly scattering nature of the ceramic composites.

Using a blue LD positioned at 30 ° incident to the phosphor, three collection angles of 0°, 45°, and 90° were used to characterize the nature of the reflected blue light. It was observed that after the normal routine of surface sanding to remove the graphite foil present after SPS preparation, the 50% Ce:YAG ceramics display Lambertian reflection of incoming laser light. This is shown quantitatively in polar coordinates in Figure 8(a), which leads to diffuse blue reflection that mixes with yellow Ce:YAG emission to create white light (Figure 8(c)). A Ce:YAG single crystal was subjected to the same sanding regime as the SPS ceramics in an attempt to create a matte surface, but under LD excitation, the single crystal displays spread blue reflection associated with a rough surface. This is shown quantitatively in Figure 8(b), where the highest peak intensity of blue light is observed at

the reflected angle of 30°, leading to a spread laser spot surrounded by a halo of converted yellow light (Figure 8(d)). It is likely that the high hardness of the Ce:YAG single crystal prevented sufficient roughening using the techniques attempted in the present work. However, it is difficult to conclude that surface roughening alone would prevent total internal reflection in the single crystal phosphor. Therefore, effort needs to be taken to texture or pattern the surface of single crystals in the attempt to produce Lambertian reflection of blue light, whereas SPS-prepared polycrystalline ceramics in the present work display Lambertian emission as prepared without additional processing, resulting in high outputs of thermally stable white light. Therefore, the increased thermal conductivity of ceramic composites over single crystals, as well as the Lambertian scattering achieved with no additional sample preparation render ceramic composites competitive candidates for high power LD-based lighting devices in reflection geometries.

4 Conclusions

The realization of encapsulation-free phosphor ceramics is required for the next generation of laser-based white lighting due to the temperature limitations of resins and glasses. With increased light output, drastically lower operating temperatures, and white color points, these composites offer an advantage over the exemplary phosphor material alone. By mixing α-Al_2O_3 and Ce:YAG powders and consolidating using SPS, the steady state operating temperature of the ceramic under laser flux is observed to reduce greatly. This is likely due to the presence of less phosphor material, as well as the thermal conductivity of α-Al_2O_3 being larger than Ce:YAG single crystals by a factor of $\approx$3. One key advantage to using α-Al_2O_3 over other filler/composite oxides is that there are no phases between $Y_3Al_5O_{12}$ and Al_2O_3 on the Y_2O_3/Al_2O_3 phase diagram, which results in no reactivity between the two oxides during preparation of the ceramic composites. Thus, using α-Al_2O_3 prevents the formation of secondary phases, ensuring the purity of Ce:YAG in the ceramic compos-

ites produced. Improvements in efficiency will come from improvements in processing, as well as the use of higher quality starting materials with higher initial QY values. One important benefit of the SPS technique is that many oxide materials, both oxide phosphors and high thermal conductivity scattering oxide fillers, can be combined and sintered together. These scattering ceramics are viable candidates for LD-based white lighting due to the improved thermally stability, which is seen to reduce the operating temperature of the phosphors regardless of sample density in the configurations tested thereby preventing thermal quenching of the phosphor. Additionally, light is scattered and results in a more uniform distribution of blue and yellow light. For use in devices, the relationships between heat mitigation, color uniformity, and luminous flux must be considered as a function of the specific device geometry, including sample size and heat sink size, as small samples can be combined with LDs to achieve quasi-point source-like behavior.

5 Acknowledgements

The work presented herein was funded in part by the Advanced Research Projects Agency-Energy (ARPA-E), U.S. Department of Energy, under Award Number DE-AR0000671. Thanks to G. Laurita for guidance with Rietveld refinements and T. Mates for SIMS measurements. C. C. would like to thank the National Science Foundation for a Graduate Research Fellowship under Grant No. DGE 1144085. Use of the Advanced Photon Source, an Office of Science User Facility operated for the U.S. Department of Energy (DOE) Office of Science by Argonne National Laboratory, was supported by the U.S. DOE under Contract No. DE-AC02-06CH11357. Use of the Shared Experimental Facilities of the Materials Research Science and Engineering Center at UCSB (MRSEC NSF DMR 1720256) is gratefully acknowledged. The UCSB MRSEC is a member of the NSF-supported Materials Research Facilities Network (www.mrfn.org).

6 Supporting Information

Laser radiant power and wall plug efficiency of the laser diodes used in the experiment, photographs of ceramic samples before and after annealing, and qualitative SIMS of ceramics before and after annealing.

References

(1) Wierer, J. J.; Tsao, J. Y.; Sizov, D. S. Comparison Between Blue Lasers and Light-Emitting Diodes for Future Solid-State Lighting. *Laser Photon. Rev.* **2013**, *7*, 963–993.

(2) Kuritzky, L. Y.; Speck, J. S. Lighting for the 21st Century with Laser Diodes Based on Non-Basal Plane Orientations of GaN. *MRS Commun.* **2015**, *5*, 463–473.

(3) Cantore, M.; Pfaff, N.; Farrell, R. M.; Speck, J. S.; Nakamura, S.; DenBaars, S. P. High Luminous Flux from Single Crystal Phosphor-Converted Laser-Based White Lighting System. *Opt. Express* **2016**, *24*, A215–A221.

(4) Basu, C.; Meinhardt-Wollweber, M.; Roth, B. Lighting with Laser Diodes. *Adv. Opt. Technol.* **2013**, *2*, 313–321.

(5) Lee, C.; Shen, C.; Oubei, H. M.; Cantore, M.; Janjua, B.; Ng, T. K.; Farrell, R. M.; El-Desouki, M. M.; Speck, J. S.; Nakamura, S.; Ooi, B. S.; DenBaars, S. P. 2 Gbit/s Data Transmission from an Unfiltered Laser-Based Phosphor-Converted White Lighting Communication System. *Opt. Express* **2015**, *23*, 29779–29787.

(6) Lee, C.; Zhang, C.; Cantore, M.; Farrell, R. M.; Oh, S. H.; Margalith, T.; Speck, J. S.; Nakamura, S.; Bowers, J. E.; DenBaars, S. P. 4 Gbps Direct Modulation of 450 nm GaN Laser for High-Speed Visible Light Communicationirect modulation of 450 nm GaN laser for high-speed visible light communication. *Opt. Express* **2015**, *23*, 16232–16237.

(7) Lee, C.; Shen, C.; Cozzan, C.; Farrell, R. M.; Speck, J. S.; Nakamura, S.; Ooi, B. S.; DenBaars, S. P. Gigabit-Per-Second White Light-Based Visible Light Communication Using Near-Ultraviolet Laser Diode and Red-, Green-, and Blue-Emitting Phosphors. *Opt. Express* **2017**, *25*, 17480–17487.

(8) Cozzan, C.; Brady, M. J.; O'Dea, N.; Levin, E. E.; Nakamura, S.; DenBaars, S. P.; Seshadri, R. Monolithic Translucent $BaMgAl_{10}O_{17}:Eu^{2+}$ Phosphors for Laser-Driven Solid State Lighting. *AIP Adv.* **2016**, *6*, 105005.

(9) Birkel, A.; Denault, K. A.; George, N. C.; Doll, C. E.; Hery, B.; Mikhailovsky, A. A.; Birkel, C. S.; Hong, B.-C.; Seshadri, R. Rapid Microwave Preparation of Highly Efficient Ce^{3+}-Substituted Garnet Phosphors for Solid State White Lighting. *Chem. Mater.* **2012**, *24*, 1198–1204.

(10) George, N. C.; Denault, K. A.; Seshadri, R. Phosphors for Solid-State White Lighting. *Annu. Rev. Mater. Res.* **2013**, *43*, 481–501.

(11) Dorenbos, P. Thermal Quenching of Eu^{2+} 5d–4f Luminescence in Inorganic Compounds. *J. Phys. Condens. Matter* **2005**, *17*, 8103.

(12) Bachmann, V.; Ronda, C.; Meijerink, A. Temperature Quenching of Yellow Ce^{3+} Luminescence in YAG:Ce. *Chem. Mater.* **2009**, *21*, 2077–2084.

(13) Ueda, J.; Dorenbos, P.; Bos, A. J.; Meijerink, A.; Tanabe, S. Insight into the Thermal Quenching Mechanism for $Y_3Al_5O_{12}:Ce^{3+}$ Through Thermoluminescence Excitation Spectroscopy. *J. Phys. Chem. C.* **2015**, *119*, 25003–25008.

(14) Fujita, S.; Yoshihara, S.; Sakamoto, A.; Yamamoto, S.; Tanabe, S. YAG Glass-Ceramic Phosphor for White LED (I): Background and Development. Opt. Photonics 2005. 2005; pp 594111–594117.

(15) Kim, E.; Unithrattil, S.; Sohn, I. S.; Kim, S. J.; Chung, W. J.; Im, W. B. Facile One-Step Fabrication of 2-Layered and 4-Quadrant Type Phosphor-in-Glass Plates for White LEDs: an Insight into Angle Dependent Luminescence. *Opt. Mater. Express* **2016**, *6*, 804–814.

(16) Arjoca, S.; Víllora, E. G.; Inomata, D.; Aoki, K.; Sugahara, Y.; Shimamura, K. Ce:$(Y_{1-x}Lu_x)Al_5O_{12}$ Single-Crystal Phosphor Plates for High-Brightness White LEDs/LDs with High-Color Rendering (R_a>90) and Temperature Stability. *Mater. Res. Express* **2014**, *1*, 25041.

(17) Frage, N.; Kalabukhov, S.; Sverdlov, N.; Ezersky, V.; Dariel, M. P. Densification of Transparent Yttrium Aluminum Garnet (YAG) by SPS Processing. *J. Eur. Ceram. Soc.* **2010**, *30*, 3331–3337.

(18) He, L.-f.; Fan, G.-h.; Lei, M.-y.; Lou, Z.-l.; Zheng, S.-w.; Su, C.; Xiao, Y.; Chen, Z.-w.; Zhang, T. Luminescent Properties of New $MgAl_2O_4$/CeYAG Transparent Ceramics for White LED Applications. *Chinese J. Lumin.* **2013**, *2*, 3.

(19) Shen, L.; Li, Y.; Huang, Q. Ultrafast Fabrication of Solid Phosphor Based White Light Emitting Diodes: From Powder Synthesis to Devices. *Appl. Phys. Lett.* **2013**, *103*, 121908.

(20) Li, S.; Zhu, Q.; Tang, D.; Liu, X.; Ouyang, G.; Cao, L.; Hirosaki, N.; Nishimura, T.; Huang, Z.; Xie, R.-J. Al_2O_3–YAG:Ce Composite Phosphor Ceramic: a Thermally Robust and Efficient Color Converter for Solid State Laser Lighting. *J. Mater. Chem. C.* **2016**, *4*, 8648–8654.

(21) Mueller-Mach, R.; Mueller, G. O.; Krames, M. R. Phosphor-Converted High Power LEDs. Manufacturing LEDs for Lighting and Display. 2007; pp 67970G–67970G.

(22) Raukas, M.; Kelso, J.; Zheng, Y.; Bergenek, K.; Eisert, D.; Linkov, A.; Jermann, F. Ceramic Phosphors for Light Conversion in LEDs. *ECS J. Solid State Sci. Technol.* **2013**, *2*, R3168–R3176.

(23) Chaim, R.; Marder-Jaeckel, R.; Shen, J. Z. Transparent YAG Ceramics by Surface Softening of Nanoparticles in Spark Plasma Sintering. *Mater. Sci. Eng. A* **2006**, *429*, 74–78.

(24) Chaim, R.; Kalina, M.; Shen, J. Z. Transparent yttrium Aluminum Garnet (YAG) Ceramics by Spark Plasma Sintering. *J. Eur. Ceram. Soc.* **2007**, *27*, 3331–3337.

(25) Sakata, S.-I.; Mitani, A.; Fujii, I. *Light Conversion Structure and Light-Emitting Device Using the Same*; 2011.

(26) Sai, Q.; Zhao, Z.; Xia, C.; Xu, X.; Wu, F.; Di, J.; Wang, L. Ce-Doped Al_2O_3-YAG Eutectic and its Application for White LEDs. *Opt. Mater.* **2013**, *35*, 2155–2159.

(27) Tang, Y.; Zhou, S.; Chen, C.; Yi, X.; Feng, Y.; Lin, H.; Zhang, S. Composite Phase Ceramic Phosphor of Al_2O_3-Ce:YAG for High Efficiency Light Emitting. *Opt. Express* **2015**, *23*, 17923–17928.

(28) Yoshimura, M.; Sakata, S.-i.; Iba, H.; Kawano, T.; Hoshikawa, K. Vertical Bridgman Growth of Al_2O_3/YAG:Ce Melt Growth Composite. *J. Cryst. Growth* **2015**, *416*, 100–105.

(29) Song, Y. H.; Ji, E. K.; Jeong, B. W.; Jung, M. K.; Kim, E. Y.; Lee, C. W.; Yoon, D. H. Design of Laser-Driven High-Efficiency Al_2O_3/YAG:Ce^{3+} Ceramic Converter for Automotive Lighting: Fabrication, Luminous Emittance, and Tunable Color Space. *Dyes Pigm.* **2017**, *139*, 688–692.

(30) Larson, A. C.; Von Dreele, R. B. GSAS. *General Structure Analysis System. LANSCE, MS-H805, Los Alamos, New Mexico* **1994**,

(31) Toby, B. H. EXPGUI, a Graphical User Interface for GSAS. *J. Appl. Crystallogr.* **2001**, *34*, 210–213.

(32) Leyre, S.; Coutino-Gonzalez, E.; Joos, J.; Ryckaert, J.; Meuret, Y.; Poelman, D.; Smet, P.; Durinck, G.; Hofkens, J.; Deconinck, G.; Hanselaer, P. Absolute Determination of Photoluminescence Quantum Efficiency Using an Integrating Sphere Setup. *Rev. Sci. Instrum.* **2014**, *85*, 123115.

(33) Morita, K.; Kim, B.-N.; Yoshida, H.; Hiraga, K.; Sakka, Y. Influence of Pre-and Post-Annealing on Discoloration of $MgAl_2O_4$ Spinel Fabricated by Spark-Plasma-Sintering (SPS). *J. Eur. Ceram. Soc.* **2016**, *36*, 2961–2968.

(34) Baker, R. T. K.; Sherwood, R. D.; Derouane, E. G. Further Studies of the Nickel/Graphite-Hydrogen Reaction. *J. Catal.* **1982**, *75*, 382–395.

(35) Abell, J.; Harris, I.; Cockayne, B.; Lent, B. An Investigation of Phase Stability in the Y_2O_3-Al_2O_3 System. *J. Mater. Sci.* **1974**, *9*, 527–537.

(36) Sai, Q.; Xia, C. Tunable Colorimetric Performance of Al_2O_3-YAG:Ce^{3+} Eutectic Crystal by Ce^{3+} Concentration. *J. Lumin.* **2017**, *186*, 68–71.

(37) Denault, K. A.; Cantore, M.; Nakamura, S.; DenBaars, S. P.; Seshadri, R. Efficient and Stable Laser-driven White Lighting. *AIP Adv.* **2013**, *3*, 072107.

(38) Shi, H.; Chen, J.; Huang, J.; Hu, Q.; Deng, Z.; Cao, Y.; Yuan, X. Preparation and Luminescence Properties of YAG:Ce Phosphor for White LED Application via a Vacuum Sintering Method. *Phys. Status Solidi A* **2014**, *211*, 1596–1600.

(39) Bechtel, H.; Schmidt, P. J.; Tücks, A.; Heidemann, M.; Chamberlin, D.; Müller-Mach, R.; Müller, G. O.; Shchekin, O. Fully Phosphor-Converted LEDs with Lumiramic Phosphor Technology. SPIE Optical Engineering + Applications. 2010; pp 77840W–77840W.

(40) Zelmon, D. E.; Small, D. L.; Page, R. Refractive-Index Measurements of Undoped Yttrium Aluminum Garnet From .4 to 5.0 μm. *Appl. Opt.* **1998**, *37*, 4933–4935.

(41) Kirchstetter, T. W.; Novakov, T.; Hobbs, P. V. Evidence That the Spectral Dependence of Light Absorption by Aerosols Is Affected by Organic Carbon. *J. Geophys. Res.* **2004**, *109*.

(42) Chen, Y.; Bond, T. Light Absorption by Organic Carbon from Wood Combustion. *Atmos. Chem. Phys.* **2010**, *10*, 1773–1787.

(43) Chen, J.; Lan, H.; Cao, Y.; Deng, Z.; Liu, Z.; Tang, F.; Guo, W. Application of Composite Phosphor Ceramics by Tape-casting in White Light-emitting Diodes. *J. Alloys Compd.* **2017**, *709*, 267–271.

(44) Schubert, E. F. *Light Emitting Diodes*; Wiley Online Library, 2006.

(45) Munro, R. G. Evaluated Material Properties for a Sintered Alpha-Alumina. *J. Am. Ceram. Soc.* **1997**, *80*, 1919–1928.

(46) Francl, J.; Kingery, W. Thermal Conductivity: IX, Experimental Investigation of Effect of Porosity on Thermal Conductivity. *J. Am. Ceram. Soc.* **1954**, *37*, 99–107.

(47) Leung, V.; Lagendijk, A.; Tukker, T.; Mosk, A.; IJzerman, W.; Vos, W. Interplay Between Multiple Scattering, Emission, and Absorption of Light in the Phosphor of a White Light-Emitting Diode. *Opt. Express* **2014**, *22*, 8190–8204.

Graphical TOC Entry

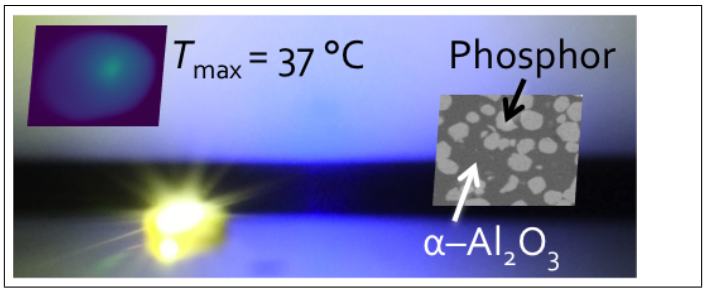

Supporting Information for Stable, Heat Conducting Phosphor Composites for High-Power Laser Lighting

Clayton Cozzan,[†,‡,¶] Guillaume Lheureux,[‡] Nicholas O'Dea,[‡] Emily E. Levin,[†,¶] Jake Graser,[§] Taylor D. Sparks,[§] Shuji Nakamura,[†,‡,‖] Steven P. DenBaars,[†,‡,‖] Claude Weisbuch,[*†,‡,‖] and Ram Seshadri[*†,‡,¶,⊥]

†Materials Department, University of California Santa Barbara, California 93106, United States

‡Solid State Lighting and Energy Electronics Center, University of California Santa Barbara, California 93106, United States

¶Materials Research Laboratory, University of California Santa Barbara, California 93106, United States

§Department of Materials Science and Engineering, University of Utah Salt Lake City, Utah 84112, United States

‖Department of Electrical and Computer Engineering, University of California Santa Barbara, California 93106, United States

⊥ Department of Chemistry and Biochemistry, University of California Santa Barbara, California 93106, United States

E-mail: weisbuch@engineering.ucsb.edu; seshadri@mrl.ucsb.edu

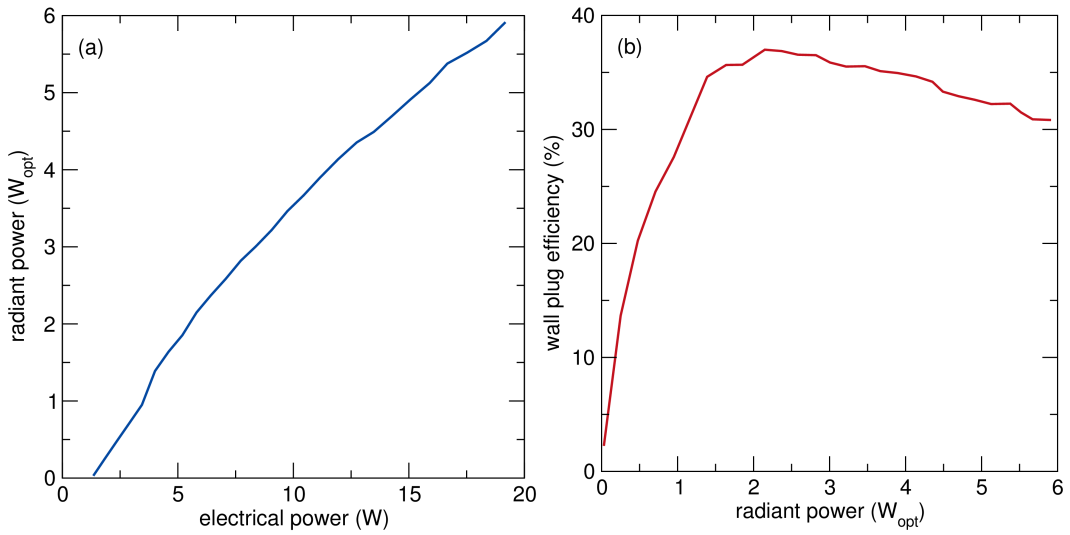

Figure S1: (a) Laser radiant power (W) versus electrical power (W) and (b) laser wall plug efficiency (%) as a function of radiant power (W) shown right for the commercial laser diodes employed in the present work.

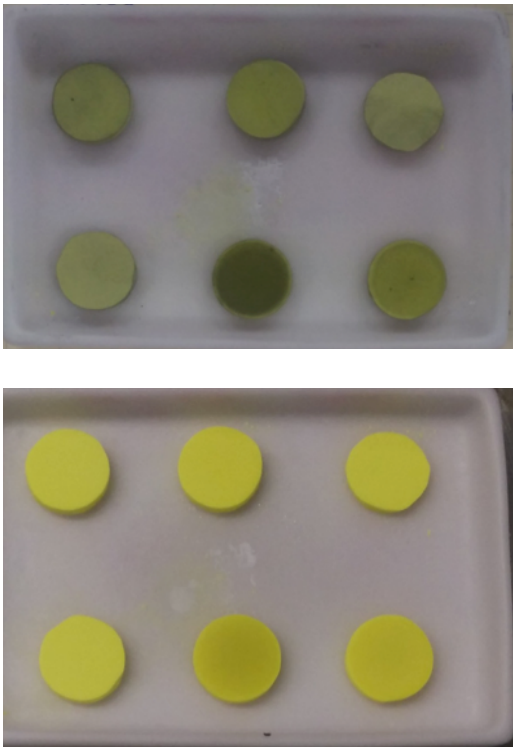

Figure S2: Photographs of samples after spark plasma sintering and removing the graphite foil (top), followed by a subsequent annealing step (bottom) of 2 °C/min to 1500 °C for 24 h with a 2 °C/min cool to room temperature. Sample density was not altered by the annealing step.

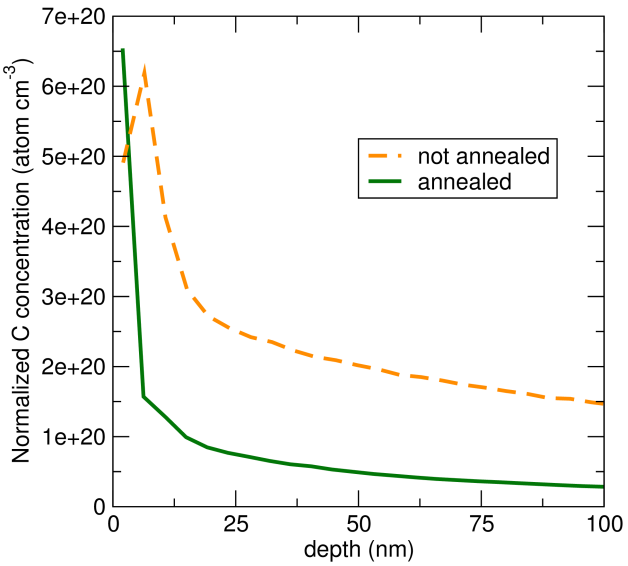

Figure S3: Qualitative SIMS data shows higher levels of carbon for the not annealed sample. SIMS ionization efficiency for an arbitrary system were used to estimate absolute carbon concentration. However, carbon still exists in the annealed sample. Removing carbon in future processing will therefore increase efficiency.

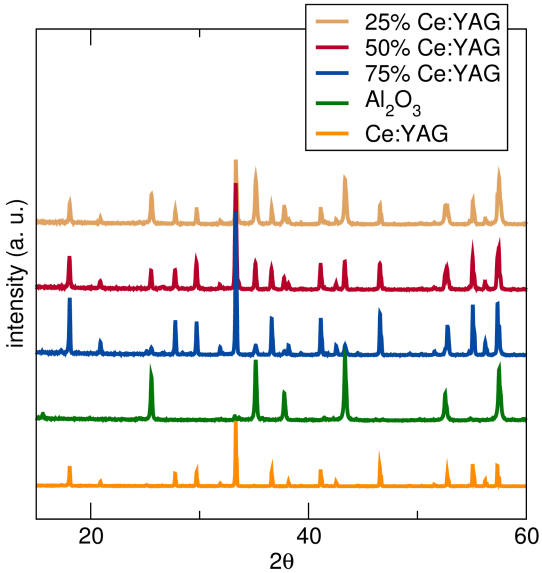

Figure S4: X-ray diffraction patterns of Ce:YAG, Al_2O_3, and 25% Ce:YAG, 50% Ce:YAG, and 75% Ce:YAG ceramic composites are shown. No intermediate phases were observed.

Table S1: Refined unit cell parameters for the 50wt% Ce:YAG ceramic composite.

	$Y_3Al_5O_{12}$ (YAG)	α-Al_2O_3 (corundum)
Cell length *a*	12.01660(8)	4.76093(7)
Cell length *b*	12.0166	4.760937
Cell length *c*	12.0166	13.0037(4)
Cell angle α (°)	90	90
Cell angle β (°)	90	90
Cell angle γ (°)	90	120
Cell volume (Å^3)	1735.180(35)	255.260(7)
Symmetry	cubic	trigonal
Space group	Ia-3d	R-3c

Table S2: Refined atomic positions for the 50 wt% Ce:YAG ceramic composite.

	x	*y*	*z*	U_{iso}
YAG				
Al1	0	0	0	0.005
Al2	0.375	0	0.25	0.005
Y1	0.125	0	0.25	0.005
O1	-0.03205	0.05414	0.15075	0.005
α-Al_2O_3				
Al1	0	0	0.35216	0.00393
O1	0.3061	0	0.25	0.00418